Aerospace Science and Technology, 1998, no. 3, 167–176

On the Practical Application of the PSE Approach to Linear Stability Analysis

M. Langlois [a], G. Casalis [b]*, D. Arnal [b]

[a] Chaire J.-A. Bombardier, École Polytechnique de Montréal, Montréal, Québec, Canada
[b] ONERA, CERT, BP 4025, 31055 Toulouse cedex, France

(Received 23 January 1997; accepted 6 June 1997)

Langlois M., Casalis G., Arnal D., *Aerospace Science and Technology*, 1998, no. 3, 167–176.

Abstract

The transition to turbulence of the laminar boundary layer plays an important role in airfoil design. The new PSE approach is more accurate and consistent than the classical Orr–Sommerfeld theory. The aim of this paper is to prove that this approach can be routinely used in practical applications to study instabilities and to predict the onset of laminar–turbulent transition. The main difficulty in its intensive use concerns the initialisation. However, systematic studies can be conducted and the results presented show that the non-parallel effects are negligible for streamwise instabilities and strengthen n factor values for crossflow instabilities. In some intermediate cases, the PSE results exhibit large crossflow amplification for low frequencies as well as large streamwise amplification at higher frequencies, whereas only the latter one is dominant according to the Orr–Sommerfeld theory. In these particular cases, the fluctuation spectra present two relative maxima (with the PSE) and the instability type and the most amplified frequencies can therefore be very different from those predicted by the Orr-Sommerfeld theory. © Elsevier, Paris

linear stability / PSE approach / application

Résumé

Applications pratiques de l'approche PSE. La position de la transition laminaire–turbulent de la couche limite joue un rôle important dans les performances aérodynamiques d'un avion. De nombreuses études ont été du reste consacrées à l'estimation de cette position. La plupart d'entre elles utilisent la théorie classique d'Orr–Sommerfeld. La nouvelle approche dite PSE est plus générale et plus précise que cette dernière et l'objectif de cet article consiste précisément à démontrer que cette approche PSE peut être utilisée de façon systématique, pour des applications pratiques comme la détermination de la position de la transition dans une couche limite tridimensionnelle. La difficulté principale pour cette utilisation « industrielle » réside dans l'initialisation des calculs. Certaines précautions étant prises, l'article présente un large éventail de cas d'applications de cette approche. Entre autres résultats, on montre que les effets non parallèles modélisés par l'approche PSE et non pris en compte par l'approche classique sont presque négligeables pour une instabilité longitudinale, mais peuvent conduire à une augmentation signification du facteur n pour une instabilité transversale. Ainsi, certains cas, a priori dominés par l'instabilité longitudinale à la lumière de la théorie classique apparaissent, par l'approche PSE, relever plutôt de l'instabilité transversale ou même, dans certains cas, de ces deux types d'instabilité. Les spectres de fluctuation présentent alors deux bosses longitudinales (avec l'approche PSE), l'une à basse fréquence correspondant à l'instabilité transversale, l'autre à haute fréquence, trace de l'instabilité. On en conclut que le type d'instabilité, ainsi que la gamme des fréquences les plus amplifiées peuvent varier considérablement avec la prise en compte des effets non parallèles. © Elsevier, Paris

stabilité linéaire / approche PSE / application

* Correspondence and reprints

Nomenclature

x	direction normal to the leading edge, in the plane of the wing
y	direction normal to the wing surface
z	direction parallel to the leading edge, in the plane of the wing
$\vec{Q}_\infty$	freestream velocity
U, V, W	mean flow velocity components in the x, y and z directions
U_∞, W_∞	freestream velocity components in the x, and z directions
u, v, w	perturbation components in the x, y and z directions
R	body curvature radius (m)
f	dimensional frequency (Hz)
α_r	wavenumber in the x direction
α_i	spatial amplification rate in the x direction
β	wavenumber in the z direction
δ_1	boundary layer displacement thickness in the x direction
λ	dimensional wavelength (m)
σ	dimensional amplification rate (m^{-1})
ψ	wave propagation orientation, with respect to the external streamline

Subscripts

e	value at the boundary layer edge
ini	value at initialisation station
tr	value at the x-location of transition
w	value at the wall
i	imaginary part
r	real part

Superscript

*	dimensional quantity

1. Introduction

The prediction of the location of transition from a laminar flow to a turbulent one plays a fundamental role in the analysis of the flowfield around most configurations of engineering interest. The linear stability theory, in its 'classical', Orr–Sommerfeld (OS) form, has been extensively used for that purpose. One of the main assumptions of this theory is that the boundary layer can be considered as locally-parallel, i.e. the mean flow is independent of x, the longitudinal direction. The influence of this hypothesis has been studied for a number of years with different approaches. In most cases, though, these approaches have been applied to the two-dimensional flat-plate flow for which the non-parallel effects are indeed small.

The more recent approach based on the Parabolised Stability Equations (PSE), originally developed by Herbert and Bertolotti [5] and Dallman et al. [7], takes into account the dominant non-parallel effects in the mean flow, as well as in the perturbed quantities. This method can easily be applied to more complex flows, such as that about a swept wing, for which the non-parallel effects are not known a priori. In the work presented here, the PSE approach was used to investigate the non-parallel linear stability of the flow over such configurations of practical interest.

2. Methodology

2.1. Parallel Stability Theory (Orr–Sommerfeld)

The main element of linear stability theory is the decomposition of all flow variables into a mean and a fluctuating part, which, for an arbitrary quantity ϕ^*, can be written as

$$\phi^*(x^*, y^*, z^*, t^*) = \Phi^*(x^*, y^*, z^*) + \tilde{\phi}^*(x^*, y^*, z^*, t^*) \quad (1)$$

In the above equation, Φ^* represents the mean flow and $\tilde{\phi}^*$ the perturbation, as the superscript * denotes a dimensional quantity. This decomposition is substituted into the governing flow equations, which, after elimination of the known mean flow and linearisation, yieds a homogenous and linear system of equations for $\tilde{\phi}^*$.

In the Orr–Sommerfeld theory, it is furthermore assumed that the mean flow is parallel, i.e. its variations in x^* and z^*, as well as its normal velocity component V^*, are neglected. Under these assumptions, the perturbation can be defined in modal form. Furthermore, using dimensionless variables the perturbation becomes

$$\tilde{\phi}(x, y, z, t) = \Re(\hat{\phi}(y)\, e^{i(\alpha x + \beta z - \omega t)}) \quad (2)$$

and appears thereby as the product of an amplitude function and an exponential term. The numbers α, β and ω are a priori complex. In this work, the spatial formulation is used, with the hypothesis that $\beta_i = 0$. Therefore, β and ω are real numbers while α is a complex number, the real part of which represents a wavenumber and the imaginary part an amplification rate. The dimensional wavelength and the wave orientation are defined respectively as

$$\lambda = \frac{2\pi}{\sqrt{\beta^{*2} + \alpha_r^{*2}}} \quad (3)$$

and

$$\psi = \tan^{-1}\frac{\beta}{\alpha_r} - \psi_e \tag{4}$$

where ψ_e is the orientation of the external streamline with respect to the x-direction. The Orr–Sommerfeld theory results in the solution of a local eigenvalue problem. The latter can be formally represented by

$$L_{OS}\hat{\phi} = 0 \tag{5}$$

The OS results presented in this paper were obtained using the code COCIP [4].

2.2. Non-Parallel Stability Theory (PSE)

The PSE approach is also based on the decomposition given by equation (1), but the x^*-independence of the mean flow, amplitude functions and wavenumber α^* is no longer assumed (this also implies that the mean flow normal component V^* is no longer neglected). It is assumed instead that these quantities exhibit a weak dependence on x^* and the form of the perturbation becomes

$$\tilde{\phi}^*(x^*, y^*, z^*, t^*) = \Re\,\hat{\phi}^*(x^*, y^*)\, e^{i\left(\int_{x_0^*}^{x^*} \alpha^*(\xi^*)\,d\xi^* + \beta^* z^* - \omega^* t^*\right)} \tag{6}$$

The PSE theory retains the z^*-independence, its strict validity is therefore limited to infinite swept wings. Rather than an eigenvalue problem, the linearised Navier–Stokes equations now lead to an x^*-evolution problem. This problem has the following form

$$L_{OS}\hat{\phi}^* + M\frac{\partial}{\partial x^*}\hat{\phi}^* + L_{NP}\hat{\phi}^* = 0 \tag{7}$$

where L_{OS} is the same operator that was present in equation (5). The operator L_{NP} contains non-parallel terms linked to the mean flow and to the term $d\alpha^*/dx^*$.

In equation (6), the x^*-dependence of the perturbation is split between the amplitude functions and the exponential term containing $\alpha^*(x^*)$. To determine α^* uniquely, a normalisation relation, imposing the slow variation in x^* of the amplitude functions, is used. Because a space-marching procedure is used, an initial solution (perturbation profiles and α^*) must be imposed in addition to the usual boundary conditions of vanishing perturbations at the wall and in the freestream. These initial conditions are provided by a parallel (OS) solution, thereby inducing a transient phase in x^*.

A PSE code was developed by the first author to produce the results that will be presented. The formulation and structure implemented in the PSE code developed at DERAT [1] have been adopted.

2.3. Transition prediction

The amplification rates calculated by the linear stability theory can be related to the transition position by the use of the e^n method. Whether the parallel or non-parallel theory is considered, the n factor is calculated by integrating the dimensional spatial amplification rate, σ, for a given dimensional frequency, f. In the parallel theory, σ corresponds to α_i^*. Different integration strategies arise from the fact that, with f fixed, there still remains the wavenumber β^* to be determined [3]. Two such strategies were considered in this work with the parallel theory: the envelope method, in which β^* is determined in such a way as to maximize the amplification rate at each position

$$n(f, x^*) = \int_{x_0^*}^{x^*} \max_{\beta^*}\{-\sigma(f, \beta^*, \xi^*)\}\,d\xi^* \tag{8}$$

and the constant-β^* method

$$n(f, x^*) = \max_{\beta^*}\left\{\int_{x_0^*}^{x^*} -\sigma(f, \beta^*, \xi^*)\,d\xi^*\right\} \tag{9}$$

in which the dimensional wavenumber β^* plays the same role as the frequency. The latter method requires that calculations must be performed for a considerable number of values of β^* at each frequency.

In the non-parallel approach, only the constant-β^* method is considered. However, the physical amplification rate, σ, and other physical properties of the perturbation such as its wavelength and orientation, are not uniquely defined but depend on what physical quantity is considered in the definition of the perturbation amplitude. In the results that follow, three amplitudes are considered, based on the maximum rms values of the two perturbation velocity components parallel to the surface and the integrated fluctuation kinetic energy

$$\begin{aligned} A_u(x^*) &= \max_{y^*}|\tilde{u}^*(x^*, y^*)|_{rms} \\ A_w(x^*) &= \max_{y^*}|\tilde{w}^*(x^*, y^*)|_{rms} \\ A_e(x^*) &= \sqrt{\int_0^\infty (|\tilde{u}^*(x^*, y^*)|^2_{rms} + |\tilde{v}^*(x^*, y^*)|^2_{rms} + |\tilde{w}^*(x^*, y^*)|^2_{rms})\,dy^*} \end{aligned} \tag{10}$$

3. Practical aspects of a PSE application

To illustrate some of the important features of the use of the PSE method for linear stability analysis, calculations were performed on three different geometries:

—an infinite swept wing with the ONERA D profile (chord normal to the leading edge, $c = 0.35$ m) in the (60, –4) configuration (sweep angle of 60° and incidence of –4°), at freestream velocities of 50, 65 and 80 $m \cdot s^{-1}$;

—an infinite swept wing with the AFVD 82 profile (chord normal to the leading edge, $c = 0.3$ m) in the (49, –2) configuration at a freestream velocity of 85 $m \cdot s^{-1}$;

—a generic wing equipped with suction chambers.

A detailed presentation of the stability results obtained can be found in reference [6]. The external velocity distributions for these three cases are shown in *figures 1–3*. On the ONERA D wing, *figure 1* indicates

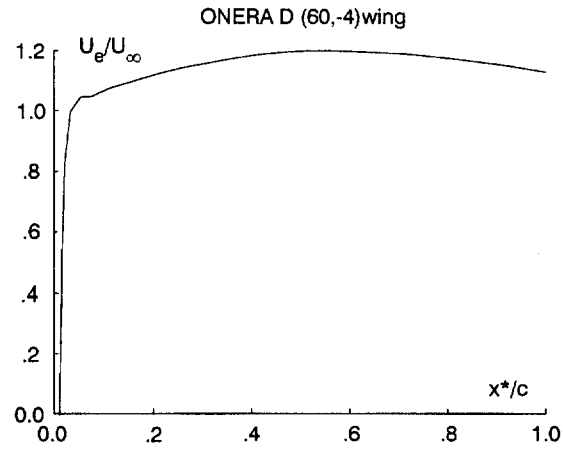

Figure 1. ONERA D (60, –4); external velocity distribution.

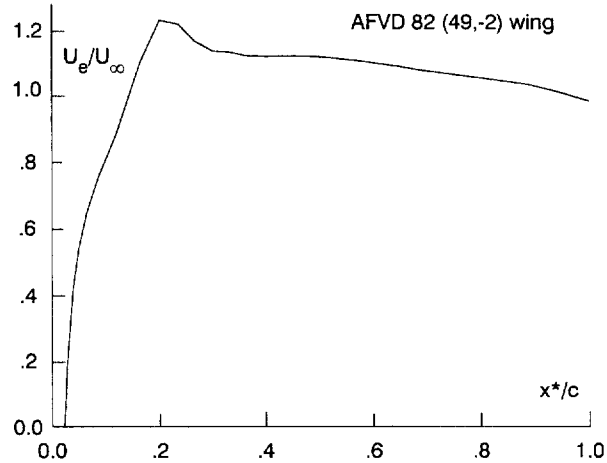

Figure 2. AFVD 82 (49, –2); external velocity distribution.

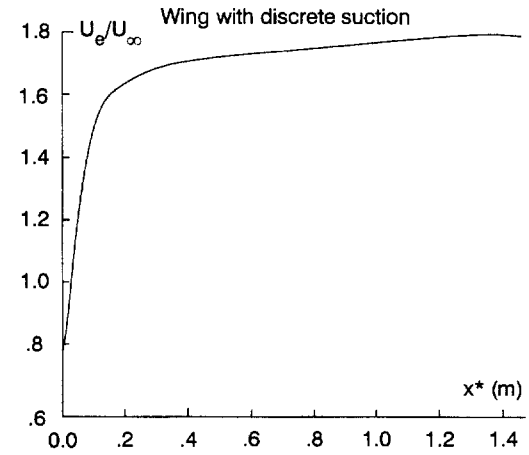

Figure 3. Wing with suction; external velocity distribution.

that streamwise instabilities will be dominant at low speeds, while crossflow or mixed disturbances will start playing a more important role as the freestream velocity is increased. The same conclusions can be drawn for the AFVD 82 wing, with a note of caution related to the rapid decrease of velocity at about quarter-chord. Finally, the continuously-increasing velocity on the wing with suction, *figure 3*, indicates that the stability of this flow will be dominated by crossflow disturbances. *Figure 4* shows the suction distribution used, with a constant suction rate in each of the chambers.

3.1. Initialisation

The initialisation is a crucial part of PSE calculations: it needs to be done in the initial region of stable flows but neither too close (for the transient to resolve) nor too far (as this induces too large an initial transient) from the neutral curve, as will be illustrated in the following example. One may know the location of the parallel neutral curve from prior OS calculations, but the location of the non-parallel

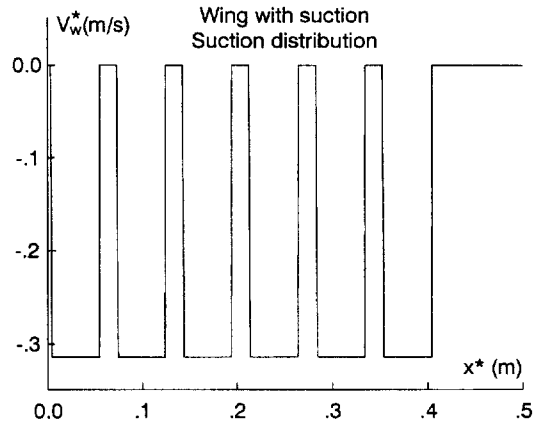

Figure 4. Wing with suction; suction distribution.

neutral curve can sometimes be significantly upstream of the former. To illustrate this, a set of calculations in which the initialisation station was varied was performed on the ONERA D wing with a freestream velocity of 80 m·s^{-1}, at the values of the frequency and wavenumber β^* associated with the most amplified wave. The results of these calculations are presented in *figure 5*. There is a range of initialisation positions in which the n factor curves coalesce, but moving out of this range, in either direction, can induce significant differences on the value of the n factor. In particular, the long-dash curve ($x^*_{\rm ini}/c = 0.0386$) corresponds to starting the PSE calculations just slightly ahead of the parallel neutral curve: at the location of transition ($x^*_{\rm tr}/c = 0.35$) this results in the n factor going down from 5.7 to 4.2. As the location of the neutral curve varies for different values of f or β^*, it is usually not possible to initialise the calculations for a complete critical range of these parameters at a single location, and the initialisation procedure has to be broken down into sub-ranges of f and β^* at different locations.

3.2. Curvature effects

As in the Orr–Sommerfeld theory, inclusion of curvature effects in the PSE only requires the modification of some terms in the stability equations, but it does not change anything in the formulation of the problem, its complexity or the computational effort necessary to its solution. It should be noted though that curvature-related terms are first-order, as they depend on the inverse of the curvature radius, which in turn is proportional to the x-derivative of the airfoil surface slope. Whereas retaining these terms is consistent with the principle of the PSE approach, where a slow variation in x of the flow properties is assumed, it may be considered inappropriate within the framework of the Orr–Sommerfeld theory.

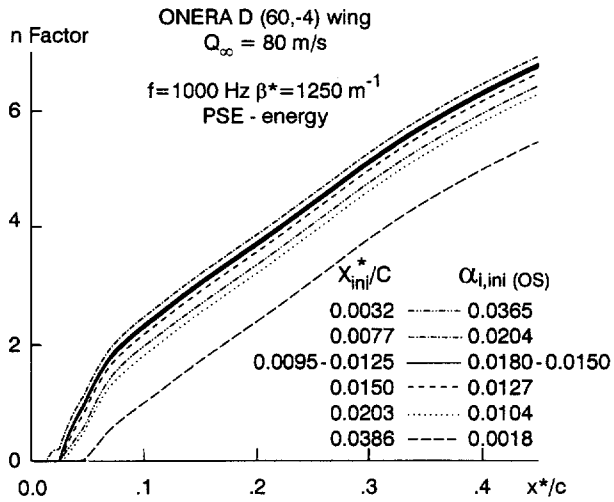

Figure 5. ONERA D (60, –4), $Q_\infty = 80$ m·s^{-1}; initialisation influence.

It is also interesting to point out that the value of the curvature radius alone does not determine the magnitude of the curvature stabilizing influence. It is rather the boundary-layer-thickness-to-radius ratio that is the determining parameter, and curvature effects are therefore not necessarily greater where the curvature ratio is smaller (i.e. very close to the leading edge). This is illustrated in *figures 6* and *7* for the ONERA, $Q_\infty = 80$ m·s^{-1}, test case at the values of frequency and β^* associated to the most amplified wave: the evolution of $\Delta\sigma$ (energy-based amplification rate difference due to curvature effects) closely follows that of the δ_1/R ratio.

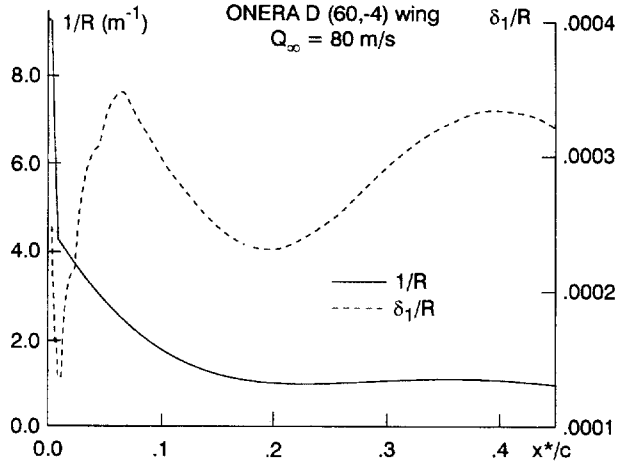

Figure 6. ONERA D (60, –4), $Q_\infty = 80$ m·s^{-1}; curvature.

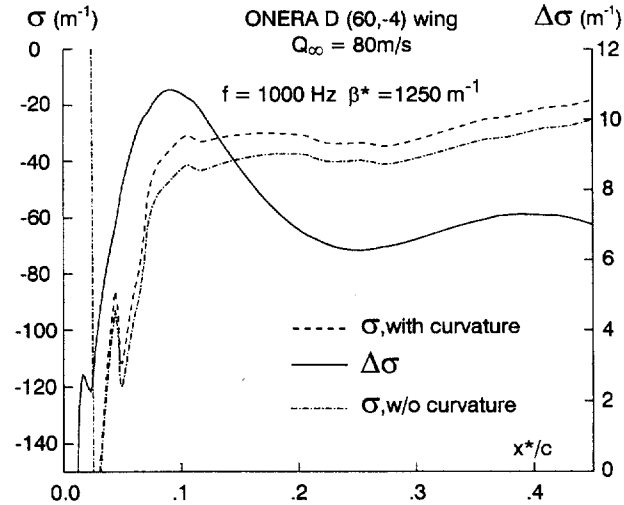

Figure 7. ONERA D (60, –4), $Q_\infty = 80$ m·s^{-1}; curvature effects.

3.3. Flows with rapid variations in x

The external velocity distribution of the ONERA D (60, –4) test case, *figure 1*, shows a small plateau

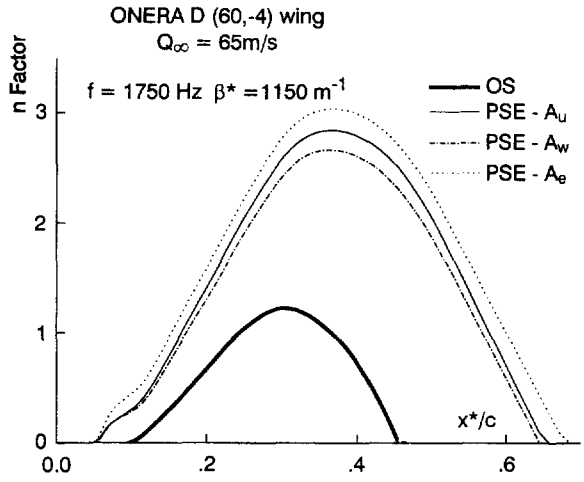

Figure 8. ONERA D (60, –4), $Q_\infty = 65\ \mathrm{m{\cdot}s^{-1}}$; n factor.

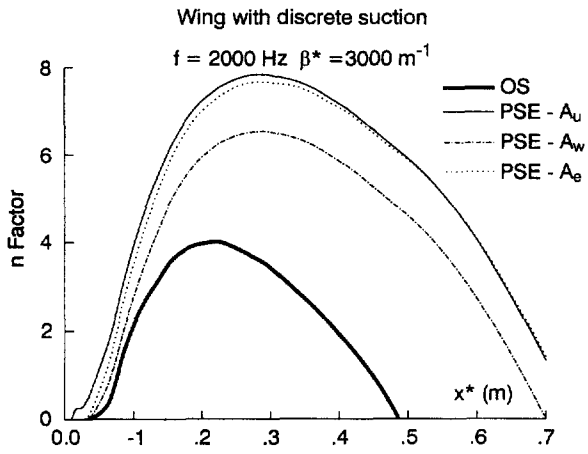

Figure 9. Wing with suction; n factor.

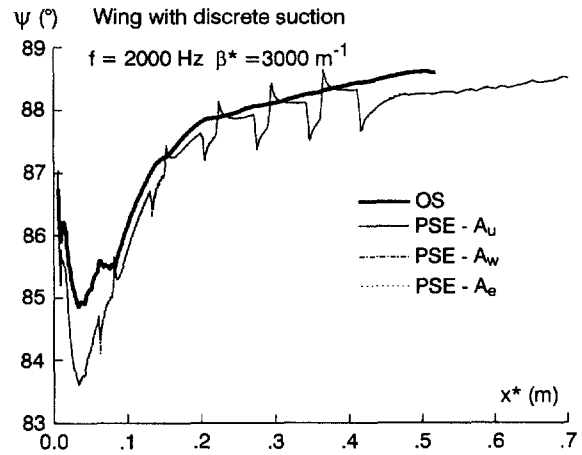

Figure 10. Wing with suction; wave orientation.

at $x^*/c \simeq 0.05$. This should result in a change of the slope of the n-factor curve, as crossflow instabilities will be locally damped by the flat pressure distribution. It is a well-known result that the OS method adapts well to these local variations (even though some numerical convergence difficulties can occur). *Figure 8* shows that this behaviour is equally well reproduced by the PSE.

Another exemple of a flow with sudden variations in x is provided by the discrete suction case. *Figure 9* presents the n factors obtained for a single frequency and spanwise wave-number. These results show that this difficult test case is handled as well by the PSE as by the OS approach. The evolution of the wave orientation for the same case is presented in *Figure 10*. The OS results are compared to the PSE results corresponding to each of the amplitudes given by equation (10). This shows a greater sensitivity of the PSE to the variations of the suction rate, the peaks on the wave orientation curves corresponding to the beginning and end of suction chambers.

The influence of the x-discretisation on the PSE results is illustrated for this same test case on *figure 11* which shows the n factors obtained when using every 'x-skip$^{\mathrm{th}}$' boundary-layer data point in the calculations. It must be noted that the base x-discretisation does not correspond to the inviscid-flow mesh, but to a finer one built by the boundary layer solver and adapted to the streamwise pressure gradient. There is no difference between using all data points or every other one, but significant differences appear if a large x-increment is used, and these come not only from the integration of the n-factor but also from differences in the amplification rates. It should be noted that this test case certainly represents an extreme, as far as the x-step requirements are concerned. In cases that do not exhibit such sudden x-variations, it is possible to use every third or fourth point or an even coarser mesh and still get the same results as with a very fine discretisation. It should also be pointed out that there

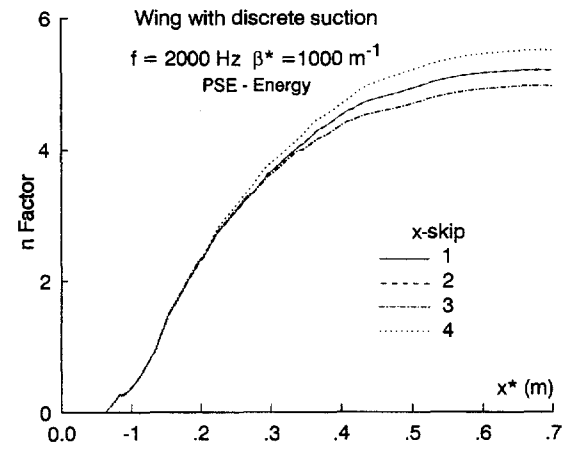

Figure 11. Wing with suction; influence of x-step.

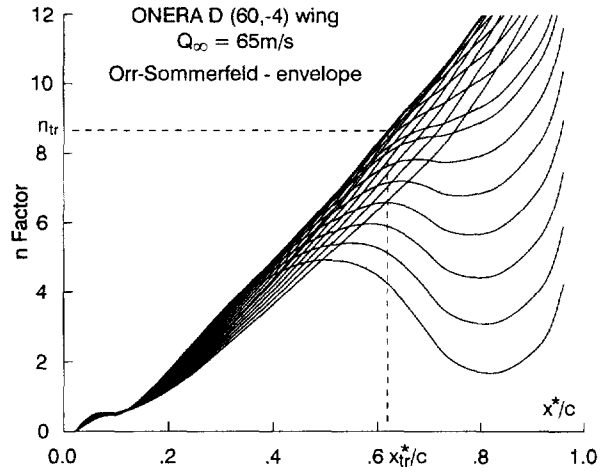

Figure 12. ONERA D (60, –4), $Q_\infty = 65$ m·s^{-1}; n factor, OS envelope.

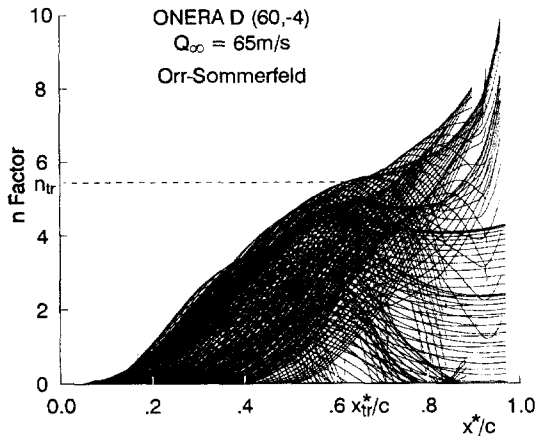

Figure 13. ONERA D (60, –4), $Q_\infty = 65$ m·s^{-1}; n factor, OS constant-β^*.

exists a theoretical lower limit for the Δx step [1], but the problem of too small a Δx has not been encountered in the practical applications presented.

3.4. Integration strategies—transition prediction

Figures 12–14 show the typical results of a linear stability analysis using the Orr–Sommerfeld and PSE approaches with the envelope and constant-β^* integration strategies, for the ONERA D, $Q_\infty = 65$ m·s^{-1} test case. With the OS envelope method, *figure 12*, only the frequency needs to be varied. With the constant-β^* strategy, the range of critical values of the spanwise wavenumber β^* must also be determined for each frequency. *Figures 13* (OS) and *14* (PSE) represent the ensemble of the f and β^* values used, resulting in a global envelope for the n factor from which the value of n at transition (or vice versa) can be obtained. The constant-β^* strategy therefore requires more computational time than the envelope strategy, but is not really any harder to implement.

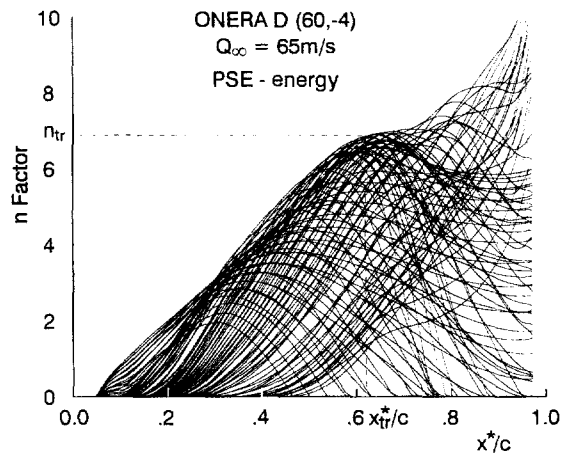

Figure 14. ONERA D (60, –4), $Q_\infty = 65$ m·s^{-1}; n factor, PSE.

4. Non-parallel effects on transition prediction

Arnal and Juillen [2] have conducted a thorough experimental investigation of the stability of the flow on the ONERA D (60, –4) and AFVD 82 (49, –2) wings, including the determination of the location of transition. This allowed a correlation of the numerical results obtained with the OS envelope, OS constant-β^* and PSE methods. For all these methods, the following results have been obtained without curvature. The results of this correlation are summarized in *tables 1–3*. *Table 1* presents the value of the n factor at the experimental location of transition. The critical values of frequency are listed in *table 2* while *table 3* indicates the orientation of the disturbance at transition.

At a freestream velocity of 50 m·s^{-1}, the stability of the flow on the ONERA D wing is dominated by streamwise disturbances, as can be seen from *table 3*. The values of the n factor at the experimentally determined location of transition, *table 1*, clearly indicate that the non-parallel effects are negligible in this case: the value of n_{tr} determined by the OS constant-β^* method falls within the range of values obtained by considering different amplitudes in the PSE. It can also be noted that the envelope method produces a much higher value of n_{tr} than both constant-β^* methods.

At $Q_\infty = 65$ and 80 m·s^{-1}, where the most unstable perturbation is neither purely streamwise nor crossflow, the non-parallel effects are more important, and of the same order of magnitude. It is interesting to note in *table* 3 that the non-parallel effects in the $Q_\infty = 80$ m·s^{-1} case cause a shift in the orientation of the dominant instability from a mixed to a purely crossflow one. *Figure* 15 shows that crossflow

Table 1. n factor at transition.

	ONERA D (60, –4)			AFVD 82 (49, –2) $Q_\infty = 85\ \mathrm{m{\cdot}s^{-1}}$ $x^*_{\mathrm{tr}}/c = 0.22$
	$Q_\infty = 50\ \mathrm{m{\cdot}s^{-1}}$ $x^*_{\mathrm{tr}}/c = 0.95$	$Q_\infty = 65\ \mathrm{m{\cdot}s^{-1}}$ $x^*_{\mathrm{tr}}/c = 0.62$	$Q_\infty = 80\ \mathrm{m{\cdot}s^{-1}}$ $x^*_{\mathrm{tr}}/c = 0.35$	
OS envelope	12.8	8.4	5.8	9.4
OS β^*	8.5	5.4	4.0	9.2
PSE — A_e	9.0	6.9	5.7	11.9
PSE — A_u	8.8	6.9	5.3	12.0
PSE — A_w	8.2	6.6	5.1	11.0

Table 2. Critical frequency (Hz).

	ONERA D (60, –4)			AFVD 82 (49, –2) $Q_\infty = 85\ \mathrm{m{\cdot}s^{-1}}$ $x^*_{\mathrm{tr}}/c = 0.22$
	$Q_\infty = 50\ \mathrm{m{\cdot}s^{-1}}$ $x^*_{\mathrm{tr}}/c = 0.95$	$Q_\infty = 65\ \mathrm{m{\cdot}s^{-1}}$ $x^*_{\mathrm{tr}}/c = 0.62$	$Q_\infty = 80\ \mathrm{m{\cdot}s^{-1}}$ $x^*_{\mathrm{tr}}/c = 0.35$	
OS envelope	1000	1400	3250	5000
OS β^*	1000	1750	3000	4000
PSE — A_e	1000	1750	1000	5000
PSE — A_u	1000	1750	1000	5000
PSE — A_w	1000	1500	1000	5000

Table 3. Wave orientation at transition (°).

	ONERA D (60, –4)			AFVD 82 (49, –2) $Q_\infty = 85\ \mathrm{m{\cdot}s^{-1}}$ $x^*_{\mathrm{tr}}/c = 0.22$
	$Q_\infty = 50\ \mathrm{m{\cdot}s^{-1}}$ $x^*_{\mathrm{tr}}/c = 0.95$	$Q_\infty = 65\ \mathrm{m{\cdot}s^{-1}}$ $x^*_{\mathrm{tr}}/c = 0.62$	$Q_\infty = 80\ \mathrm{m{\cdot}s^{-1}}$ $x^*_{\mathrm{tr}}/c = 0.35$	
OS envelope	25	25	31	72
OS β^*	16	44	49	82
PSE — A_e	14	53	84	78
PSE — A_u	11	53	84	78
PSE — A_w	13	61	84	78

instabilities are present in the parallel results (they produce the n factor maximum at $x^*/c \simeq 0.05$) but are quickly damped out and do not play any role further downstream. The inclusion of non-parallel effects results in a strengthening of these crossflow instabilities at all frequencies, *figures 16* and *17*. At the higher frequencies, though, the crossflow instabilities are still masked by the streamwise ones at the location of transition. On the other hand, at low frequencies, they retain high levels of amplification and come to dominate. In this particular case, two maxima can be observed in the fluctuation spectrum at a given position, one corresponding to a streamwise instability ($f = 3000$ Hz) and the other one to a crossflow instability ($f = 1000$ Hz).

For the AFVD 82 test case, *table 3* indicates that transition is caused by a crossflow instability whether or not the non-parallel effects are included. The non-parallel effects are very strong: *table 1* shows an increase of the n factor at transition approximately equal to 2.5, from the parallel to the non-parallel results. Contrary to previous results, the envelope method in this case produces a n factor at transition that is very close to that obtained with the OS constant-β^* method.

These results indicate that whereas non-parallel effets are negligible on streamwise instability, they are significant on mixed streamwise/crossflow disturbances and can indeed be very strong on purely crossflow ones. In some cases where the parallel theory predicts a streamwise instability to be dominant, inclusion of non-parallel effects can cause a crossflow instability to dominate. When this happens, there results a change in the critical values of the

frequency, as indicated in *table 2* for the ONERA D $Q_\infty = 80$ m·s^{-1} test case. When the nature of the dominant instability is not affected by the non-parallel effects, these values remain essentially the same (for the same integration strategy).

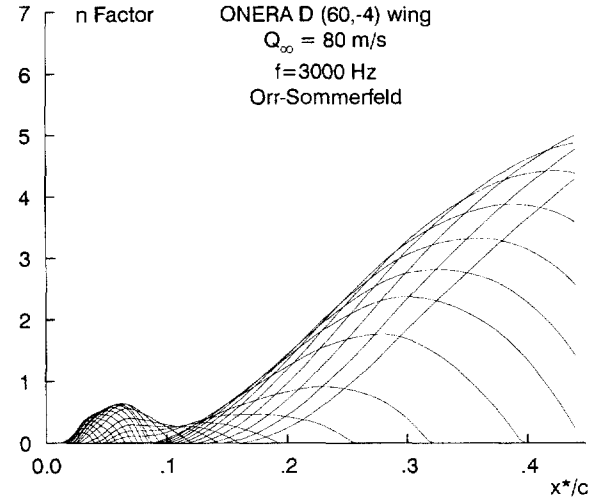

Figure 15. ONERA D (60, −4), $Q_\infty = 80$ m·s^{-1}; n factor, $f = 3000$ Hz, OS.

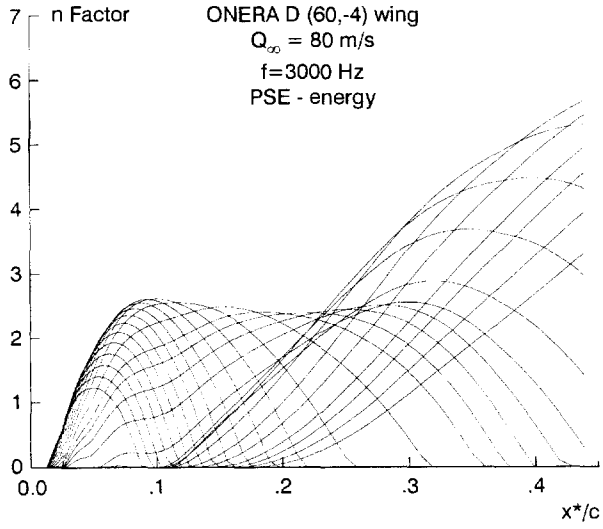

Figure 16. ONERA D (60, −4), $Q_\infty = 80$ m·s^{-1}; n factor, $f = 3000$ Hz, PSE.

5. Conclusion

As it takes into account the largest non-parallel terms, the PSE approach is more accurate than the classical OS theory. However, accuracy often requires numerical efforts and/or difficulties. The goal of the present paper was to prove that this rule is only partly true for the PSE approach. However, the examples chosen were limited to wind tunnel experiments. The applicability of the PSE approach for free-flight experiments is currently investigated within the European EUROTRANS project.

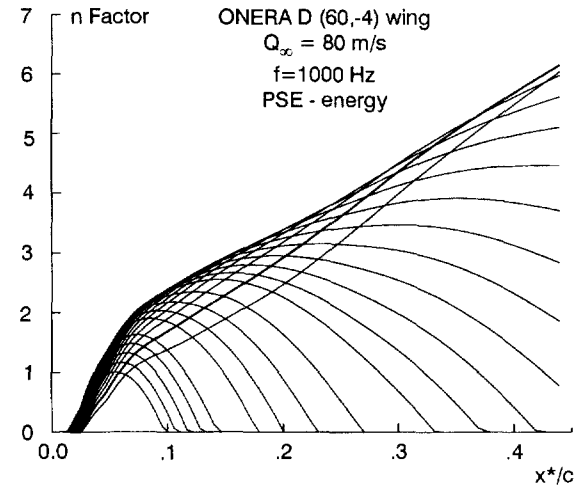

Figure 17. ONERA D (60, −4), $Q_\infty = 80$ m·s^{-1}; n factor, $f = 1000$ Hz, PSE.

From a numerical point of view, it must first be said than the CPU time required by the OS and PSE approaches is very similar. The PSE method does not present any particular convergence problem even in 'difficult' cases, such as the one with discontinuous suction presented in this article. The most important difficulty for the PSE, and maybe the only serious one, lies in the choice of the initialisation location, when the initialisation is done with OS results. As proven in this paper, there is a domain in x upstream of the OS neutral curve in which the results are independent of this location. However, in the practical use of this approach, a large number of spanwise wavenumbers and frequencies must be considered. The difficulty is then to divide this number of β^* and f into different groups and to find the proper initialisation location for each group. This problem could be partly alleviated by using results from a non-parallel local method (such as the multiple-scale analysis) to initialise the PSE.

From a theoretical point of view, the PSE approach is more general and more consistent as far as curvature effects are concerned. The effects of the non-parallel terms are negligible for streamwise instabilities and can be very important for crossflow instabilities. When both types of instability are present, the PSE results often exhibit two maxima in the fluctuation spectra at fixed x-positions. This behaviour can be verified with experimental results.

As for the practical and accurate prediction of the transition location, there is at this point no clear advantage of the PSE approach over the OS method, as none provides a consistent value of the n-factor at transition. The solution may lie in a better

understanding of the non-linear stability processes, where the PSE approach would likely be at a decisive advantage.

Acknowledgements

The Stability/Transition Research Project at École Polytechnique de Montréal is funded by a grant from the Natural Science and Engineering Research Council of Canada, in collaboration with Bombardier Inc./Canadair. The first author would like to acknowledge the support of the Fonds FCAR (Gov. of Québec) in the form of an Aerospace Graduate Scholarship and a 'Mobility Grant' which allowed the 'stage' at ONERA/CERT during which this work was conducted.

References

[1] Airiau C., Stabilité linéaire et faiblement non-linéaire d'une couche limite laminaire incompressible par un système d'équations parabolisé (PSE), PhD, These, ENSAE, Toulouse, 1994.

[2] Arnal D., Juillen J.C., Three-dimensional transition studies at ONERA/CERT, AIAA Paper 87–1335, 1987.

[3] Arnal D, Boundary layer transition: predictions based on linear theory, AGARD Report 793, 1993.

[4] Casalis G., Résolution de l'équation d'Orr–Sommerfeld en tridimensionnel et en incompressible par une méthode de Galerkin avec les polynômes de Chebichev : le code COCIP, Rapport technique DERAT 46/5618, ONERA/CERT, 1989.

[5] Herbert T., Bertolotti F.P., Analysis of nonparallel boundary layers, Bull. Am. Phys. Soc. 32, 1987.

[6] Langlois M., Casalis G, Étude détaillée des effets non parallèles sur la stabilité linéaire d'écoulements incompressibles sur une aile en flèche d'envergure infinie, Rapport technique DERAT 118/5618.24, ONERA/CERT, 1996.

[7] Simen M., Bertolotti F.P., Hein S., Hannifi A., Henningson D., Dallmann U., Nonlocal and nonlinear instability theory, Second Computational Fluid Dynamics Conference, Stuttgart, Germany, 5–8 September 1994 ECCOMAS.